Triplet Superconductivity in CrO$_2$

Triplet Superconductivity in CrO$_2$

Brin Verheijden

Huygens-Kamerlingh Onnes Laboratory, Leiden University
P.O. Box 9500, 2300 RA Leiden, The Netherlands

September 2, 2016

Abstract

In recent experiments on triplet superconductivity in full film CrO$_2$-based triplet spin valves a surprisingly large proximity effect was shown under an out-of-plane magnet field by Singh et al. [18] We aim to investigated this further with improved control over the current paths and magnetic non-collinearity in a new configuration. This is done by using more confined structures rather than a full film and by applying an in-plane field. We find that more control is needed over the magnetic non-collinearity required for triplet generation in in-plane experiments. A further improved design based on shape anisotropy is proposed to achieve this. Out-of-plane field measurements find a proximity effect coinciding in order of magnitude with the previously published results.

Contents

Chapter 1

Introduction

On the 10th of July in 1908 Heike Kamerlingh Onnes managed to set a new milestone in the history of science: he was the first to liquify helium at a temperature of $4K$. Using this liquid helium Kamerlingh Onnes made another discovery of great importance only a few years later: he discovered superconductivity in mercury at a temperature of $4.2K$. His scientific work inevitably lead to winning the Noble prize in 1913.

Nowadays more than a hundred years later, the knowledge of superconductivity has grown immensely. Many new and exotic effects have been discovered of which many are not yet completely understood. One of today's actively researched topics is superconductor-ferromagnet-hybrids. Within this field structures have been created in which even ferromagnets are superconducting, something earlier presumed impossible. The superconducting condensate in many of these structures is not in the conventional singlet state but in the parallel triplet states. This makes supercurrents running through these structures spin polarised.

Spin polarised supercurrents have the unique feature that they not only carry charge, in addition it is a spin-current. This makes them very useful for spintronics, the field which aims to build logical components similar to electronics based on spin. Because these structures have no resistance, they offer extremely suitable building blocks for fast spintronic operators without heat dissipation.

The field of spintronics is a young field, to which superconducting components are very new. Because of this it is important to look at efficient generators of these spin polarised triplet supercurrents. A device called triplet spin valve offers a good measure to quantify how efficient triplets can be generated. Triplet valves are unique devices in which the triplet superconductivity can be turned on and off. The critical tempera-

Introduction

ture changes between the on and off state and the larger the change the more efficient the triplet generation.

Several experiments [1], [2] on triplet spin valve structures have been done finding changes in critical temperature up to $120mK$ [3]. Then a new triplet spin valve based on the half metallic ferromagnet CrO_2 came in to play. CrO_2 turned out to make the triplet generation amazingly efficient. Not only is the change in critical temperature over an order of magnitude higher than any previous experiment, up to $1.8K$ [4], its supercurrents are 100% spin polarised as well. This thesis aims to further investigate these CrO_2-based triplet spin valves in a different device configuration.

Chapter 2

Theory

2.1 Introduction to superconductivity

Even though superconductivity was discovered in the early twentieth century, the first mathematical theory that successfully described this phenomenon was discovered over forty years later. This theory is named "Bardeen-Cooper-Schrieffer theory" [5] or BCS theory after its discoverers and describes what are now called "conventional superconductors".

BCS theory starts with the movement of electrons in a lattice. Due to Coulomb interaction the electrons will slightly attract any nearby atomic nucleus, causing a lattice vibration (phonon) as they travel through the lattice. This phonon pulls the atomic nuclei locally together which results in a small amount of positive charge following the electron. This positive charge causes a small attractive potential between the electrons in the material.

This (or any) attractive electron-electron potential is what is needed for the electrons to form so-called the Cooper pairs. These Cooper pairs have zero net momentum which is achieved by pairing two electrons with opposite k-vectors. This is shown in figure 2.1 together with the feature that makes the difference between a superconductor and a normal material: the "superconducting gap". This is a band gap placed exactly at the Fermi surface and this is the origin of superconductivity. What makes this gap different from normal insulators or metal is that the gap is exactly at the Fermi level. This means that at $T = 0K$ all the states below the gap are occupied and all the states above are unoccupied because of Pauli exclusion. In normal metals there would be some electrons in states above the gap and in conductors there would be space below the gap.

Normally a slight change in temperature, magnetic field, current or
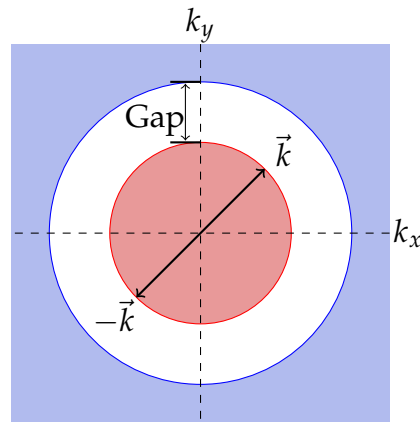
Figure 2.1: *Schematic of a Cooper pair in k-space. Red area indicates occupied states, blue area indicates free states.*

anything would easily be able to excite at least a few electrons to a higher state but this is not the case in a superconductor. All the Cooper pairs in the system share a collective wave function which follows Bose-Einstein statistics and results in what is called the superconducting condensate. In this condensate it is not possible to distinguish individual electrons or Cooper pairs, the electrons are constantly exchanged between the different pairs. This means that in order to excite one electron or electron pair, one would have to excite them all. Because of this, electron scattering is not possible; as that would mean a change in either energy or momentum. This is why superconductors have zero resistance.

The obvious way to suppress the superconductivity is to add energy. This can be done by increasing temperature, current or magnetic field. Because of this it is possible to define a critical temperature (T_C), field (H_C) and current (I_C) at which the system is superconducting, though the precise definitions may vary. The critical parameters are connected, meaning that increasing one parameter (for example the magnetic field) to nearly its critical value lowers the other critical values (in this example temperature and current).

2.2 Triplet superconductivity

Many superconducting system can not be described by BCS theory. These materials are usually called unconventional superconductors. There are several different ways in which unconventional superconductors can differ from conventional superconductors but for this thesis the this will be

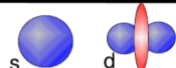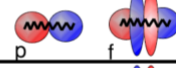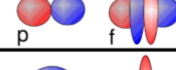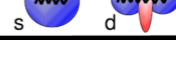limited to singlet and triplet superconductivity.

As stated earlier, since electrons are fermions Cooper pairs have to obey the Pauli exclusion principle and have an antisymmetric (odd) wave function. In conventional superconductors Cooper pairs are antisymmetric in their spin state, which is the following state:

- $|\uparrow\downarrow\rangle - |\downarrow\uparrow\rangle$ with $S = 0$ and $m_S = 0$

S is the magnitude of the spin momentum of the Cooper pair and m_S is its z-component. Because there is only one state for m_S when $S = 0$ this is called the singlet state. Besides the singlet state there are three triplet states, which have symmetric (even) spin-parts in their wave functions.

- $|\uparrow\uparrow\rangle$ with $S = 1$ and $m_S = 1$

- $|\uparrow\downarrow\rangle + |\downarrow\uparrow\rangle$ with $S = 1$ and $m_S = 0$

- $|\downarrow\downarrow\rangle$ with $S = 1$ and $m_S = -1$

Since the spin part of these Cooper pairs is even the antisymmetry of the wave function must come from either the frequency/time or the momentum. Different possible combinations are shown in figure 2.2. The superconductivity in the devices discussed in this theses are s-wave superconductivity, so the antisymmetry originates from the frequency.

Spin	Frequency	Momentum	
Singlet (odd) $\uparrow\downarrow - \downarrow\uparrow$	Even	Even	s d
	Odd	Odd	p f
Triplet (even) $\uparrow\uparrow \quad \downarrow\downarrow$ $\uparrow\downarrow + \downarrow\uparrow$	Even	Odd	p f
	Odd	Even	s d

Figure 2.2: *A table showcasing the different kinds of pairing symmetries. [6]*

2.3   Proximity effect

The proximity effect is a phenomenon that occurs at the boundaries of superconductor. Different variations of the same effect will occur for different materials but this section will only cover the boundary effects of

non-superconducting normal metals (N) and superconductors (S), the so-called S/N-systems. The superconducting condensate $\Psi(x)$ is a macroscopic quantum state, that needs to be spatially continuous. In the bulk of a superconductor it has a constant amplitude Ψ_0. In a normal metal, on the other hand, the amplitude of the wave function is zero. To make this possible there must be a change at the boundary of the superconductor. In order order to satisfy the continuity equations the condensate leaks into the normal metal and exponentially decays as function of the distance (see figure 2.3). The typical decay length is called the Ginzburg-Landau coherence length and is given by ξ.
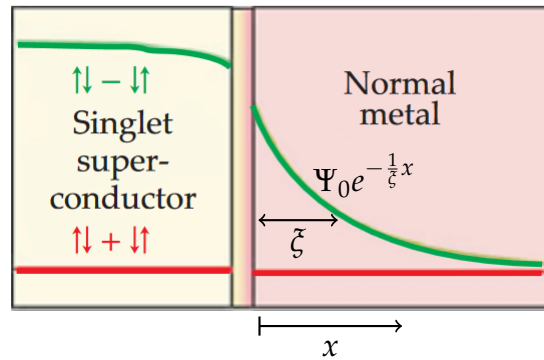
Figure 2.3: *This graph show how the superconducting condensate leaks into the normal metal. ξ is the Ginzburg-Landau coherence length. [7]*

The result of the superconducting condensate leaking into the normal metal is that the metal becomes superconducting in proximity of the superconductor.

The leaking of the superconducting condensate into the normal metal affects the superconductor too. As visible in figure 2.3 the superconducting condensate leaks out of the superconducting lowering the critical values close to the boundary. This again is an effect that exponentially decays as show in equation 2.1.

$$\Psi(x) = \Psi_0(1 - c \cdot e^{\frac{1}{\xi'}x}) \tag{2.1}$$

In which c is constant and dependent of the material and ξ' is the coherence length of the superconductor in the other direction.

2.4 Triplet generation

If one would replace the normal metal by a ferromagnet proximity occurs as well, but with a much faster decay depending on how strongly polarised the ferromagnet is. In this situation there will be an additional effect called spin mixing [8].

2.4.1 Spin mixing

Spin mixing is a direct consequence of the interaction between the exchange field (the magnetic interaction that forces ferromagnets to be parallel and anti-ferromagnets to be anti-parallel) of the ferromagnet (for simplicity this will be assumed to have one single magnetic domain) and the magnetic moments of the electrons in the Cooper pairs. From section 2.2 it is known that the spin state of a (conventional) Cooper pair is the singlet state: $|\uparrow\downarrow\rangle - |\downarrow\uparrow\rangle$. When this Cooper pair interacts with the exchange field the up and down state will be parallel and anti-parallel respectively (or the other way around, depending of the orientation of the exchange field). This difference in orientation causes a slight shift in energy and momentum, shown by figure 2.4. Because of this shift in momentum the net momentum will be non-zero. In figure 2.4 the Cooper pair will have a net momentum in the $\vec{k}_{\uparrow}$-direction.
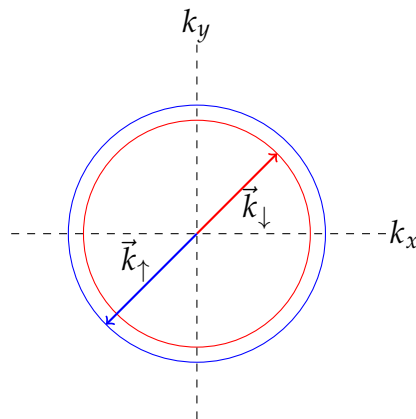
Figure 2.4: *The graph above shows the change in momentum of the Cooper pair due to the interaction between the exchange field and the electron spins. The exchange field is parallel to the $\uparrow$-state in this figure.*

The singlet state Cooper pairs are a linear combination of the $|\uparrow\downarrow\rangle$- and the $|\downarrow\uparrow\rangle$-state. The difference between these states is that in the electrons

the spins are flipped compared to their momentum. This means that the $|\downarrow\uparrow\rangle$-state has a shift in momentum of the same magnitude but in the opposite direction compared to the $|\uparrow\downarrow\rangle$, which shall be called $\vec{Q}$ and $-\vec{Q}$ respectively. Because of this the singlet state changes as shown in equation 2.2.

$$|\uparrow\downarrow\rangle - |\downarrow\uparrow\rangle \longrightarrow |\uparrow\downarrow\rangle e^{i\vec{Q}\cdot\vec{R}} - |\downarrow\uparrow\rangle e^{-i\vec{Q}\cdot\vec{R}} \tag{2.2}$$

If the x-axis is chosen to be perpendicular to Superconductor-ferromagnet interface the term in the exponent will be $e^{i\vec{Q}\cdot\vec{R}} = e^{i\phi x}$. This way we can rewrite equation 2.2 to equation 2.3.

$$|\uparrow\downarrow\rangle e^{i\phi x} - |\downarrow\uparrow\rangle e^{-i\phi x} = (|\uparrow\downarrow\rangle - |\downarrow\uparrow\rangle)\cos(i\phi x) + i(|\uparrow\downarrow\rangle - |\downarrow\uparrow\rangle)\sin(i\phi x) \tag{2.3}$$

This leave two terms, one singlet term and one triplet ($S = 1$, $m_S = 0$) term with a cosine and a sine as their coefficients respectively. Because the wave function will be squared to form a chance distribution, the state will continuously change from singlet to triplet and back as a function of x. This is where the spin gets mixed up as shown in figure 2.5.

2.4.2 Spin polarised triplets

The triplet spin states are the states with a net spin where the singlet state has zero spin. For the singlet state this implicates that any spin component one would measure would be zero as well (though, only one spin component can be measured at once due to the Heisenberg uncertainty principle). The components of triplets states can be $m_S = -1$, $m_S = 0$ and $m_S = 1$, as described section 2.2. The proximity effect in superconductor-ferromagnet structures (SF-structures) causes the $m_S = 0$ pair to be formed, as section 2.4.1 shows, but does teach anything regarding the $m_S = \pm 1$ pairs that are so important for spintronics.

For the generation of spin-polarised Cooper pairs one needs to bring the $m_S = 0$ to a ferromagnet. This can be done by adding a new ferromagnetic layer to the already existing SF-structure. Buzdin [9] was in 2007 the first one to describe these so-called SF'F''-structures. When the second ferromagnetic layer (F'') is polarised in a different direction than the first ferromagnetic layer (F') spin polarised Cooper pairs will be formed. From now on the polarisation of F' shall be called the z-axis.
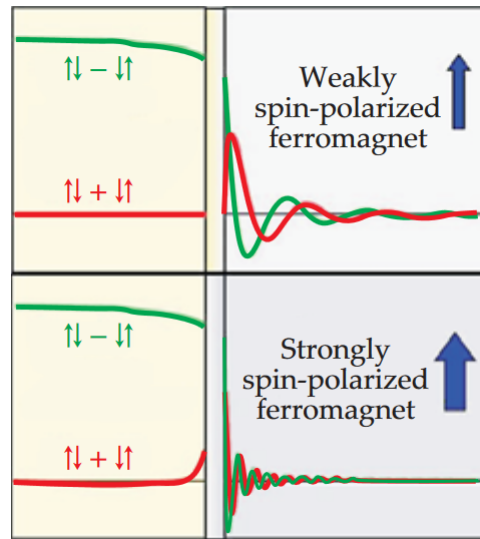
Figure 2.5: *Proximity effect and spin mixing in ferromagnets for weak and strong ferromagnets. The figure shows the combined effect of the exponential decay due to proximity effect and the oscillation due to spin mixing. The wave functions in this figure are not squared. [7]*

The $m_S = 0$ triplets do have a spin component (because $S = 1$), but not in the z-direction, in which is measured. So the spin must be somewhere in the x-, or y-direction. Due to the uncertainty principle it is not possible to know more than one component at once, so that does not help. But by placing F″ in such a way that the polarisations of F′ and F″ are perpendicular (or at least have a perpendicular component) on can start measuring in another direction (which will be called the y-axis in this section). By measuring in the y-direction one now can find the $m_S = \pm 1$ triplets. The more perpendicular the ferromagnets are, the more equal spin pairs ($m_S = \pm 1$) can be found. From the same logic it is understandable that when both ferromagnets are polarised parallel there will be no equal spin triplets, since there will be no change in observed axis. By changing the relative orientations of the ferromagnets (with for example a magnetic field) one can turn on and off the equal spin superconductivity.

Note then when these equal spin triplet pairs have been found in the y-direction, the z-component becomes unmeasurable again.

Lastly, to make these equal spin triplets fully polarised, F″ must be a half-metal. Half metals are special materials. Normal metals have a band gap below the Fermi-level, so there are electrons in the conduction band resulting in low resistance, insulators have a band gap above the Fermi-level causing all the electrons to be in the valence band resulting in high

resistance. In a half metal the band gap is different for electrons with different spins due to the magnetic properties of the material. Because of this, the material in insulating for one of the spin orientations (the minority spins) and is conducting for the other spins (the majority spins). This allows only the triplets with majority spin. Figure 2.6 shows the electron bands of the half-metal CrO_2.
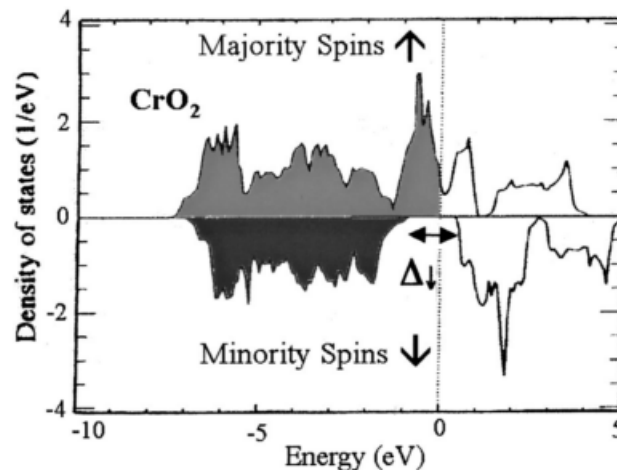
Figure 2.6: *This graph shows the difference in electron bands for the majority spins ↑ and de minority spins ↓ for the half metal CrO_2. It clearly displays a band gap that only exists for the minority spins, indicated by $\Delta_\downarrow$. Figure from [10], data from [11].*

The coherence length of these equal spin triplets in the SF'F"-structure is very long compared to the coherence length in the SF-structure. In the case of a half metal this can even get close to the coherence in a normal metal. This makes these structure very suitable for Josephson junctions. Josephson junctions are superconducting structures with a so-called weak link of a non-superconducting material. The weak link is made out of a material that normally would not be superconducting, but is due to proximity effect. This non-superconducting material has a lower critical current than the rest of the structure, hence the name "weak link". This effect is originally predicted by Josephson [12] and experimentally confirmed with a tin-tin oxide-lead junction by Anderson and Rowell [13]. Keizer [14] was the first to create a magnetic Josephson junction with CrO_2, discovering its superconducting properties with that same experiment. This junction had a remarkably high I_C, which indicates efficient triplet generation.

Keizer used a structure of only NbTiN (superconductor) and CrO_2. This is different from the SF'F'' structure described earlier in this section and by Houzet [9]. There is only one ferromagnet in this structure that full-fills the role of both the F'- and F''-layers. The non-collinearity in this structure comes from different magnetic domains in the CrO_2. In general there a few known and predicted [6] mechanisms to create long range equal spin triplets. There is the method used by Klapwijk: magnetic non-collinearity due to the intrinsic magnetic orientations of the material. Secondly, there is the typical SF'F''-system, with non-collinearity due to the orientations of the individual magnets. Lastly there is the spin-orbit coupling-to-ferromagnet method which will be described in section 2.4.4, in which SO-coupling is the spin mixing mechanism that replaces the F'-layer in the SF'F''-type structures. There are several more (predicted) mechanisms to create long range triplets, but these will not be discussed in this thesis. Even independent of what mechanism is used, the SF'F''-like structure can be built in different ways, and one way offers an immense control over the structure: the triplet spin valve.

2.4.3 Spacer layer

Up until now one small detail is overlooked in these SF'F''-structures. In theory one can choose two ferromagnets to be both adjacent to each other and have perfectly orthogonal magnetic orientations. In reality the magnetic moments interact with the exchange fields of both ferromagnets. This causes the magnetic moments at the interface to tilt towards each other, creating a finite and continuous transition space. This domain wall influences the way equal spin triplets are formed and is therefore something that should be avoided. That is what the spacer layer is used for. The spacer layer is a thin layer of normal metal that is placed between the ferromagnets to suppress their exchange fields. This layer must be thinner than the spin diffusion length of the metal. In figure 2.7 a schematic of the CrO_2 structure used for very efficient triplet generation [4] is shown.

For the spacer layer Singh had used copper, light metal with low SO-coupling. Copper has one downside: it oxidises. An alternative for copper is the noble metal silver, though this metal is slightly heavier than copper but does not oxidise, making it more suitable for the spacer layer.
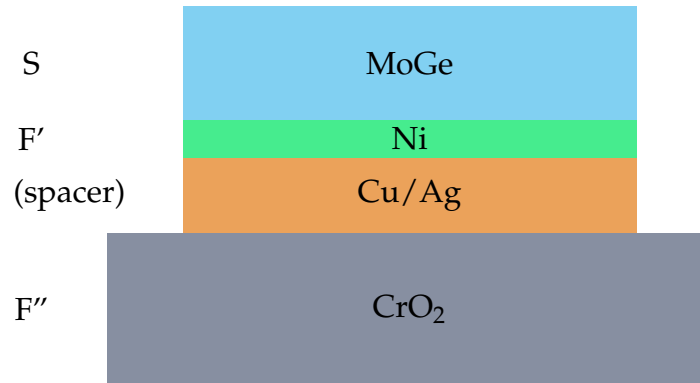
Figure 2.7: *An example of an S/F′/F″-junction, based on the device used by source [4]. In this case for the superconductor (S) molybdenum germanium (MoGe) is used, nickel (Ni) is used for the spin mixing ferromagnet (F′) and for the long range triplet layer (F″) layer chromium dioxide (CrO_2) is used. The spacer layer used by Singh was made out of copper (Cu).*

2.4.4   Spin-orbit coupling

Spin-Orbit coupling (SO coupling) is something that happens when an electron gets close to a heavy atomic nucleus. The classical (and partially incorrect) picture is that when the electron orbits around the nucleus, this can be considered a circular current. The spin moment of the electron interacts with the magnetic field, which can cause it it flip (change direction).
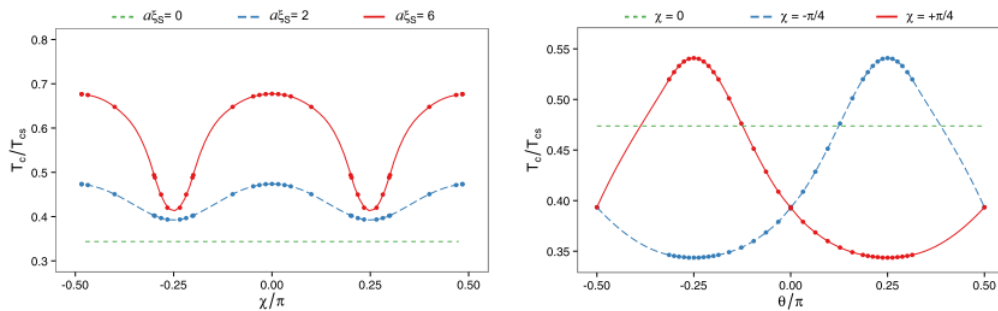
Figure 2.8: *This graph shows the change in T_C as a function of θ (the angle between the exchange field vector) and χ (the angle indicating the ratio between the Rashba and Dresselhaus SO-coupling, $\pm 45°$ means same magnitude). [15]*

In superconductivity spin orbit coupling is known to "break" Cooper pairs and therefore suppress superconductivity. The reason this happens is that spin orbit coupling changes the momentum of the electrons in the Cooper pair. Unless the momentum change is opposite for the $|\uparrow\downarrow\rangle$ com-

pared to the change for the $|\downarrow\uparrow\rangle$, this results in a quick exponential decay. On the other hand, if the changes in momentum are symmetric, this would result in normal spin mixing. According to an article by Jacobsen et al. [15], this can be achieved when the Rashba SO-coupling term is of the same order of magnitude as the Dresselhaus SO-coupling term, or ideally: exactly as large. To create long ranged triplets from this kind of spin mixing one must add another ferromagnetic layer. If now the angle θ between the exchange field and the SO-coupling vector in the plane of the superconductor-metal interface would be changed, the long range triplets can be turned "on" and "off". These kind of structures require only one ferromagnetic layer. Figure 2.8 shows how the critical temperature would change as function of θ and χ. In which χ displays the ratio between the Rashba and Dresselhaus SO-coupling ($\pm 45°$ means they have the same magnitude).

2.4.5   Triplet spin valves

Triplet spin valves (or TSV's) are superconductor-ferromagnet-ferromagnet structures in which the relative orientation of the magnetisations of the ferromagnets can be controlled. This is usually done by using two ferromagnets with a different magnetic susceptibility. When both magnets are parallel and a perpendicular field is applied both magnets turn their orientations towards the direction of the magnetic field. Because of difference in susceptibility one of the magnets responds stronger than the other and therefore turns more than the other. This creates the kind of non-collinearity that is necessary for the generation of long range triplets. If the applied field is stronger it can be used to align both magnets again, parallel to the field. By changing the field, the non-collinearity of the ferromagnets can be changed and the superconductivity can be turned "on" (perpendicular) and "off" (parallel).

Because this system has two states it can be used for several spintronic devices. Spintronics is a field that researches logical spin-driven operators and devices similar to electronics. Triplet spin valves can be used as a bit in data storage and can be used as a magnetically controllable switch.

Besides applying a magnetic field it is possible to control the preferential direction of magnets using other means. Crystal structure is a good example of this. For some ferromagnets the crystal structure has an outspoken magnetic easy axis: a direction in which the magnetisation of the material prefers to align, CrO_2 is one of these ferromagnets [16]. These materials will be less susceptible to magnetic fields perpendicular to the

easy axis (parallel to the hard axis). Shape anisotropy is another effective way to force a ferromagnet to align in a certain way. This is very dependant on the strength of the exchange field and the distance over which it carries. The shape of a ferromagnet changes the energetically optimal configuration of its magnetic domains.

Triplet spin valve devices are usually used to measure the difference in critical temperature due to the proximity effect. Because the equal spin triplets leak deep into the ferromagnet there is a large drop in critical temperature of the superconductor. Because the superconductivity can be turned on and off it is very easy to measure the strength of this effect. The size of the drop is a very good measure to for the efficiency of the triplet generation of the SF'F''-structure. The current record holder for proximity effect in a triplet spin valve is currently set using a device with CrO_2 (this device has been briefly mentioned in section 2.4.3 and figure 2.7). The change in critical temperature was measured up to $1.8K$ by Singh [4], [17]. This effect is colossal compared to the previous record of $120mK$ [17], [3] where cobalt is used. Something notable about these structures is that CrO_2 is the only half metal of which there are multiple reports on SF'F'' systems.

Though these TSV's show a colossal difference in T_C, the effect is not solely due to triplet superconductivity. Singh has done several control experiments to show that every layer in the stack is necessary to create the full $1.8K$ T_C-drop. These experiments do not exclude other mechanisms to contribute. One of these mechanisms is the magnetic field used to turn the nickel layer (ferromagnet) out-of-plane. As explained in section 2.1 an applied magnetic field lowers the critical temperature of the sample, so part of the T_C-drop is due to this effect. The fact that the field is applied out-of-plane makes room for several effect not related to triplets like vortices, which cause T_C to drop quadratically as a function of the field. Smaller, 1-dimensional structures have only give a linear drop in T_C, that transition from 2-dimensional (quadratic) to 1-dimensional is called the dimensional crossover. In-plane measurements have not been done yet to exclude these 2-dimensional effects. Another interesting detail is that the ferromagnetic layer this TSV were not fully non-collinear: simulations by Peter Sterk [18] show that the largest angle between the magnetic orientations was 30°.

The design for of Singh's colossal TSV is shown in figure 2.9. This design consists of two layers, forming an SF'F''-structure with a spacer layer: a chromium dioxide bottom and a trilayer stack on top of that. The trilayer stack is made out of a superconductor: molybdenum germanium, a spin mixing ferromagnet: nickel and copper as the spacer layer. The easy axis of CrO_2 in this figure is the horizontal axis.
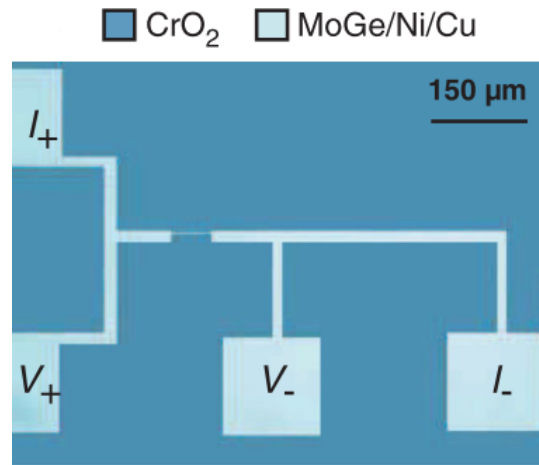
Figure 2.9: *The sample design used to create the 1.8K drop in T_C. The darker parts are CrO₂, the lighter part is a MoGe-Ni-Cu-multilayer (MoGe on top). [4]*

Figure 2.9 shows two important features in the trilayer design: the contact pads and the actual device. Since the top layer of the design is the superconductor MoGe the contact pads have no resistance, making sure that only the actual structure contributes to the measured resistance. The thin line in the middle of the design is the actual TSV. It has a rectangular shape with its long axis parallel to the easy axis of the CrO_2. The shape anisotropy forces the Ni to magnetically align parallel to the long axis (and therefore to the CrO_2 easy axis), making the natural state (0 magnetic field) of the triplet spin valve the off-state. Because the thin bar in the middle is significantly smaller then the rest of the structure all resistance (at room temperature) will be dominated by the small TSV structure. Because of this, even at 0 resistance, only the effect of the triplet spin valve will be measured.

The design is meant for the measurement of the T_C of MoGe in the on- and off-state of the TSV. The nickel in this structure is a thin film, and when thin films are under the influence of an out-of-plane field the flux through the sample becomes very relevant. This causes effects not related to triplet such as vortices that lower the critical temperature. This must be taken in account when measuring the T_C change due to triplet superconductivity. To exclude these additional effects Singh has done several control experiments with changes to break the long range triples to determine their magnitude (around $100\ mK$). For the result of $\Delta T_C = 1.8K$ these effects are taken in account.

The "colossal" triplet spin valve received criticism from a different an-

gle: because the multilayer stack was deposited on the whole structure it is very hard to control the exact current paths. The CrO_2 layer underneath might short the circuit, changing the actual current in the structure.

To completely exclude these factors the measurements should be done with an in-plane field to change the relative magnetisations.

Chapter 3

Methodology

This chapter will discuss the experimental methods used for the measurement and preparation of the TSV devices. Besides triplet spin valves a junction device will be discussed as well.

3.1 Sample design

3.1.1 Triplet spin valve
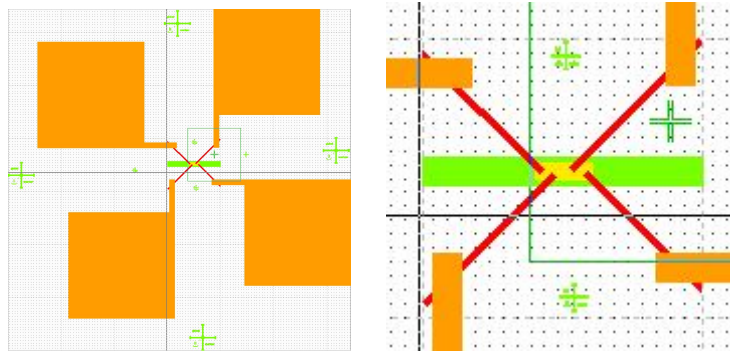
Figure 3.1: *The first design used for triplet spin valves (left) and a magnification of the central part (Right). The green parts are CrO_2, the yellow part is the MoGe-Ni-Ag/Pt trilayer and the orange and red parts are the silver contacts.*

The design (see figure 3.1 for the first version) used for this thesis has a few adaptations compared to the one Singh used. Firstly, the magnetic field will be applied in-plane to eliminate not triplet related effects. Secondly, this design will have a confined area where the multilayer stack will

be. This stack is put on a CrO_2 bar, and not a full film to exclude the possibility of shorting the structure. The spacer in the multilayer is changed from copper to silver, this because silver is less likely to react with the oxygen in CrO_2 and form an oxide layer. For one of the devices the silver is replaced with platinum, a heavy noble metal with high spin-orbit coupling. This is done because the same article [15] that predicted SO-coupling as a spin mixing suggests that high SO-coupling in the spacer layer might enhance spin mixing. The next difference is the contact pads. The contact pads are made out of silver (not a superconductor) which will be deposited directly on the multilayer in a separate layer.

This design meant to be measured for in-plane fields applied in the vertical direction (CrO_2 hard axis) of the sample. Out-of-plane field measurements can be done too, to find how much the long range triplets contribute.
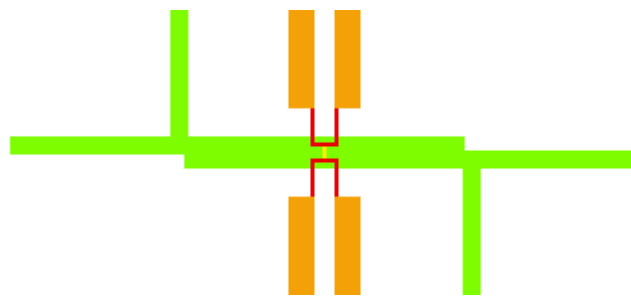
Figure 3.2: *The second triplet spin valve design. Green is CrO_2, yellow is the MoGe-Ni-Ag trilayer, orange and red are silver contacts.*

Later on a second design has been made with a change in the orientation of the trilayer as shown in figure 3.2. The important change is that the long axis of the rectangular trilayer is now in de vertical (CrO_2 hard axis) direction. In addition to this, the long/short ratio has been increased from $10 : 3$ to $10 : 1$, to make sure the nickel will be magnetically align with the vertical direction. Because of this, the natural state of this TSV is the on-state. The additional parts in the CrO_2-layer are to measure interface transparency.

3.1.2 Junction

Figure 3.3 shows a the design of a junction. This junction does not have the separate contact pads the triplet spin valves in figures 3.1 and 3.2 have they are built in with the trilayer stack.

Figure 3.3: *The design of the easy axis junction (left) and the hard axis junction (right). The green structures represent CrO$_2$, the yellow structures the MoGe-Ni-Ag trilayer.*

There are different CrO$_2$ bars in the design (the green layer in figure 3.3): horizontally aligned (easy axis bars) and vertically aligned (hard axis bars). The easy axis bars have a single junction on them, with the shape anisotropy forcing the nickel to align perpendicular to the CrO$_2$. These single easy axis junctions are meant to test whether this kind of set-up works or not.

The hard axis bars have several junctions on them to be able te measure possible different resistances of the different junctions. Since the bar is aligned along the hard axis, it will split up into several easy axially aligned domains [16]. The hard axis bar set-up can be used to measure the effects of domains and domain walls in SF'F" structures. Notable is that these structures do not have a separate layer for the contacts, these are built in with the MoGe-Ni-Ag layer. This is done because these structures do not require optimisation of proximity effect. If either of the junctions does not go superconducting in the 0 field state an out-of-plane field can be applied to create non-collinearity.

3.2   Sample preparation

The preparation of every sample mentioned in this thesis follows the same procedure. Some samples use different materials or doses, some samples skip a certain step but the preparation of each triplet spin valve is representative for the methods used for every fabricated device.

3.2.1   CrO$_2$ growth

The base of each device is a single crystal TiO$_2$ wafer with a rutile crystal structure [16]. This crystal structure is important, because it is the same structure CrO$_2$ needs to be able to grow. On this wafer a 25nm layer of silicon oxide is deposited using sputter deposition. Sputter depositing is

a process that uses plasma to etch a target of the desired material and deposit it on the sample. This is done by applying a voltage (up to $1kV$, depending on the material) between the target en the sample. Argon gas will flow through the room until it ionises and allows a current to flow between the target and sample. This process loosens particles from the target which will be deposited on the sample until the desired layer thickness is reached.
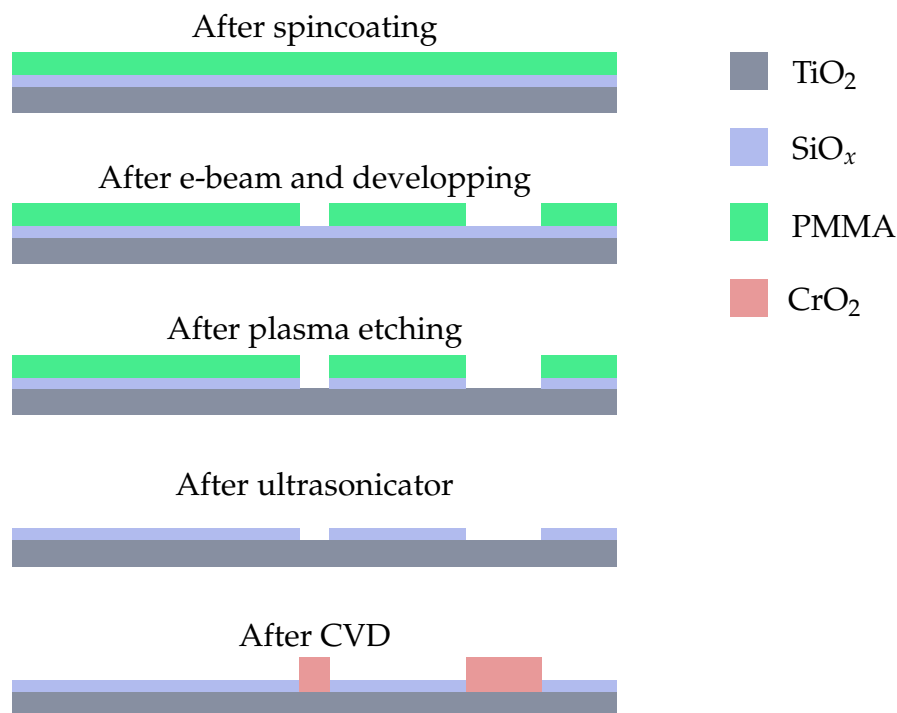

Figure 3.4: *Schematic of the different steps of the selective area growth of CrO_2.*

The SiO_x-coated TiO_2 wafer will be used for selective area growth (see figure 3.4). Selective area growth is the process of shielding parts of the TiO_2 to only allow growth on the desired places. Electron beam lithography is used to do this. The first step is spin coating the SiO_x with two layers of the positive resist PMMA (600k) and one layer of conductive polymer. The PMMA has to be baked at $180°C$ for two minutes and cooled down before the next layer can be applied. Resists are polymers that change when they are exposed to an electron beam with a dose of about $150\frac{\mu C}{cm^2}$. After this the resist will be exposed to a developer ($3 : 1$ isopropanol : MIBK, $\sim 50sec$) and part of the resist will dissolve. For a positive resist the exposed part will dissolve, for a negative resist this is the unexposed part. The wafer, partially covered with PMMA will now be

plasma etched for about $2m30$ in a $5 : 5 : 1$ mixture of Ar, CHF_3 and O_2. The argon is for physical etching, using the momentum of the plasm the etch through the SiO_x, and to clean up the reaction products of the chemical etching. Chemical etching is done with CHF_3 and O_2 and using the reactive properties of the plasma to cut through the SiO_x. These parameters have been optimised to cut through the SiO_x while leaving the TiO_2 as unharmed as possible.

After the plasma etching the polymers are cleaned off with isopropanol (IPA) and acetone in an ultrasonic bath. The next step is the chemical vapour deposition (CVD) of CrO_2. CVD happens in a chamber with two heated elements: one for the sample and one for the precursor. The precursor is CrO_3 and is heated to $260°C$ and evaporates CrO_3 into the chamber. An oxygen flow leads the vapour to the sample where it, at a temperature of $395°C$ deposits as CrO_2. This is a very delicate process that is highly sensitive to changes in temperature, causing different kinds of Cr_xO_y to form. Any deformations of the rutile structure due to overetching can cause the crystal lattice of CrO_2 to be changed as well, resulting in bad growth. When all the parameters are correct the CrO_2 will grow according to the process shown in figure 3.4. Figure 3.5 shows what a completed bar of CrO_2 should look like.
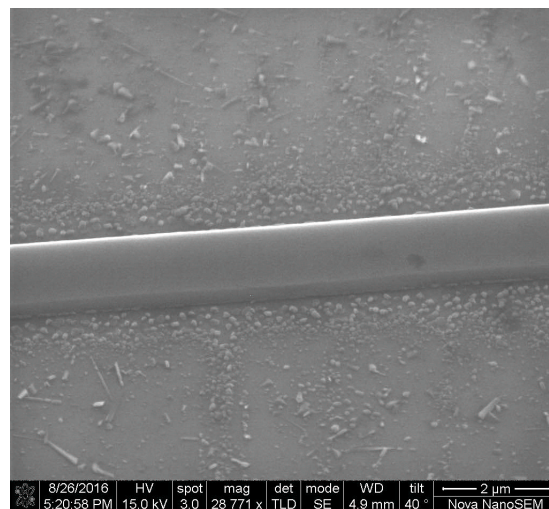
Figure 3.5: *This figure shows a SEM image of a fully grown bar of CrO_2 of high qualtity. It is approximately* $1.5\mu m$ *wide.*

Some of the samples used for this thesis use an older recipe. This consists of a trilayer of PMMA for the spin coating and CF_4 instead of CHF_3 for the plasma etching. The latter offers a greater precision, especially for

small structures [19].

3.2.2   Finishing the structure

When the CrO$_2$ is grown onto the substrate the second layer can be grown. This is again done with e beam lithography, but the spin coating recipe is slightly different this time: first one layer of PMMA 600k, then a layer of PMMA 950k and lastly another layer of conducting polymer. These layers of PMMA too need two minutes of baking at 180°C and cooling. The small green crosses visible on figure 3.1 are used to align the e-beam for high precision writing. For this type of bilayer the dose varies between the $250\frac{\mu C}{cm^2}$ and the $320\frac{\mu C}{cm^2}$, depending on the width of the structure. After developing the samples will be brought to the sputter room to deposit the trilayer of MoGe, Ni and Ag (or a variation).

Before the trilayer can be deposited it is necessary to etch the CrO$_2$. This material forms an oxide layer on its surface that is bad for the interface transparency. This is done right before sputtering the trilayer and is achieved by reversing the polarity of the sputter machine and using the sample as the sputter target for about $1m30s$. When the trilayer has been sputtered on the substrate, it will be put in acetone for several hours to dissolve the PMMA. When the PMMA is mostly dissolved like in figure 3.7, flushing the sample with acetone is used to eliminate the remaining parts of the depository residuals. This process is called lift-off and is illustrated in figure 3.6.
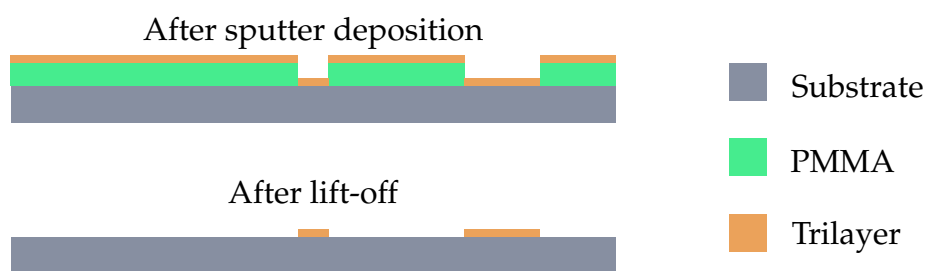
Figure 3.6: Schematic of lift-off.

If the contacts are separated from the trilayer, the last steps will be repeated from the beginning of this subsection. CrO$_2$-etching will be skipped, since that is only relevant for the interface transparency of the spacer layer. Lift-off can bring some complications as show in figure 3.8. The deposited material can stay on an area larger than intended and might need to be

(very shortly, a few seconds at most) ultrasonicated to get left of the residue. If this is done too excessively this might damage the structure.

Figure 3.7: *This figure shows what a sample (BSV8, see section 4.3.1) looks like before lift-off. The PMMA layer underneath the sputtered trilayer has been solved in acetone, that is what causes the folds.*
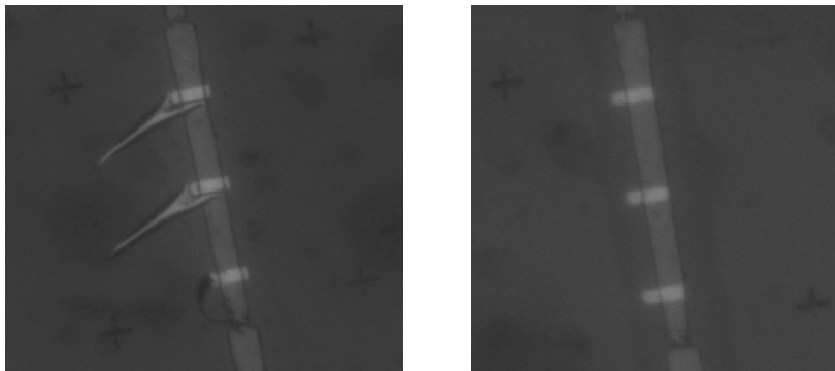
Figure 3.8: *This figure shows two structure of the sample BSV8 (see section 4.3.1). The left figure has residual metal from the lift-off, the right figure shows a structure without residue after being exposed to ultrasonic vibrations.*

If the lift-off went according to plan and the contacts are in place the sample is ready to be wired. Silver paste is used to glue the device to a PUCK that can be directly connected to the measurement software. Wire bonding itself is done with aluminium wires and wedge-shaped needle tip. The needle pushes down while vibrating sideways to melt the wire to the contacts. When the parameters (downward force, vibration amplitude and vibration time) are not optimised this can be an incredibly time consuming and frustrating effort.

3.3   Measurement techniques

The measurements are done in a cryostat called the PPMS (Physical Property Measurement System). It can apply very stable magnetic fields up to by running a current through an electromagnet that is made out of a superconducting material. By cooling it down to below the critical temperature the current is able to keep running without external voltage source so the magnetic field stays fixed at that temperature.

All used devices have MoGe as their superconductor, which goes superconducting around $6K$, depending on the specific structure. Because of this, all measurements are done at temperatures ranging between $3K$ and $7K$. By looping through field and temperature it is possible to generate data that can be used via python and internal software to create RT-curves and RH-curved. Finally, these curves will be used to determine ΔT_C.

The measurements will be done using four-point measurement, a schematic is shown in figure 3.9. The current flows from I_+ to I_- and is fixed by using a resistant R_I that is significantly higher (orders of magnitude) than the resistance of the sample R_S. This high resistance (R_I) allows the voltage used to generate the current to be constant, since the fluctuations in R_S are insignificant compared to R_I. V_+ and V_- are two probes used to measure only the voltage over R_S, there is no current between these probes. Because the voltage is separately measured from the current R_S can be very sharply measured.

The resistance of any device measured for this thesis is defined as the ratio between the voltage and current ($R = \frac{V}{I}$), not the derivative.
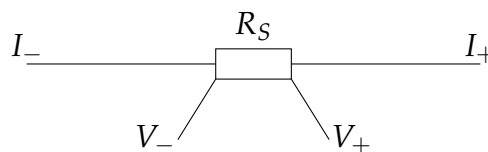
Figure 3.9: *A schematic of a circuit suitable for four point measurement.*

Chapter 4

Results

The obtained results will be presented and discussed for each device individually, in order of measurement and preparation.

4.1 BSV4: TSV with platinum spacer layer

BSV4 is a triplet spin valve using platinum for the spacer layer. It has been designed to test if platinum could be a suitable spacer layer in SF'F"-structures as predicted by Jacobsen [15].

Table 4.1: Device information of BSV4.

	Contains	**Size**
Contacts	Ag ($20 \sim 25nm$)	-
Trilayer	MoGe ($150nm$), Ni ($1.5nm$), Pt ($5nm$)	$20\mu m \times 6\mu m$
CrO_2	CrO_2	$100\mu m \times 10\mu m$

Table 4.1 shows the characteristics of BSV4. Both the CrO_2 bar and the trilayer are aligned with their long sides parallel to the CrO_2 easy axis, according to the design in figure 3.1. The CrO_2 of this sample was used using the "old" recipe briefly described in section 3.2.1: using a trilayer of PMMA (600k) and a conducting layer for the e-beam lithography and CF_4 for the plasma etching. The CrO_2 had later been etched for $1m30s$ to eliminate of the oxide layer. The contact pads are connected to the PUCK using an aluminium wire.

This design has two defining features, the first being the platinum spacer layer and the second one being the $150nm$ thick MoGe layer. The platinum layer has been chosen to be $5nm$, which is a bit on the thick

side, since the spin diffusion length of platinum is measured to be around $3 \sim 4nm$ [20]. The thickness of the MoGe is the result of a miscalculation in the sputter time of the material and as a result this makes it virtually impossible to measure large changes in T_C. For comparison: the MoGe layer used to measure Singh's colossal TSV effect had a thickness of $25nm$.
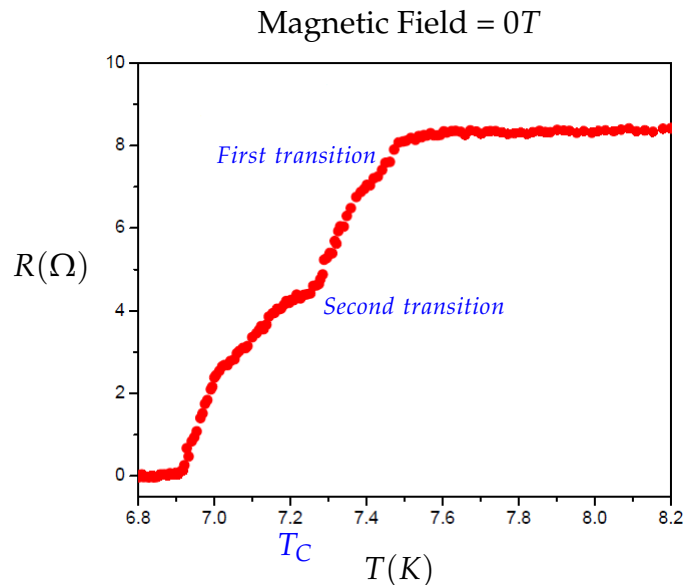
Figure 4.1: *This graph shows an RT-curve of BSV4 measured at 0 field. The used current is $15\mu A$.*

Figure 4.1 shows an RT-curve of BSV4 measured without magnetic field. The resistance of the sample starts to drop around $7.5K$ and has critical temperature of $7.2K$. The curve shows an interesting feature around $7.3K$, where the drop in resistance seems to change. This might be a result of different parts of the device going superconducting at different temperatures. The drop at $7.5K$ is likely the MoGe and the second drop ($7.3K$) could be either the triplet spin valve going superconducting or the MoGe going superconducting in an incoherent way. This second drop makes the whole transition broad, this makes it difficult to precisely determine ΔT_C. Why this transition is this broad is hard to verify but it is most likely because the MoGe layer is 7.5 times as thick as intended. Because of this the decision was made to stop measuring this device.

BSV4 was the only device not to be measured with the PPMS, another cryostat was used instead (the "7-Tesla"). There was one small downside to this, namely the temperature control. This was not completely optimised and because of that it was not very consistent in displayed temper-

ature. To save the time it would cost to optimise the temperature control all other devices have been measured using the PPMS.

4.2 BSV6: MoGe-Ni-Ag-CrO$_2$ TSV

This triplet spin valve is a variation on Singh's spin valve [4], meant to be measured in-plane. It consists of MoGe-Ni-Ag multilayer on top of the CrO$_2$ bar, both parallel to the easy axis (see design in figure 3.1). The dimensions of each layer can be found in table 4.2.

Table 4.2: Device information of BSV6.

|	**Contains**	**Size**
Contacts	Ag ($25nm$)	-
Trilayer	MoGe ($20nm$), Ni ($1.5nm$), Ag ($5nm$)	$20\mu m \times 6\mu m$ (CITATION)
CrO$_2$	CrO$_2$	$100\mu m \times 10\mu m$

This device is made using a PMMA (600k) trilayer and a conducting layer and uses CF$_4$ for plasma etching (old recipe, see section 3.2.1). The CrO$_2$ etch time is $1m30s$ and the contact pads are connected to the measurement set-up using an aluminium wire.

4.2.1 In-plane measurements

The first important step in measuring a new triplet spin valve is finding out if the device goes superconducting at all. Figure 4.2 shows how the TSV gradually goes superconducting around $5.5K$. Above the critical temperature the voltage is linearly dependant of the current, as Ohm's law would predict for any normal resistor. When the temperature approaches the critical point, the graph shows non-linearity. This non-linearity gradually becomes more visible until the graph is horizontal around zero current. This horizontal behaviour is superconductivity: the current increases without an increase in voltage.

The measurement shown in figure 4.2 is taken with an in-plane magnetic field of $15mT$. At such a magnetic field the superconducting transition is best visible at low currents. This becomes even more notable at higher field. Because of this all further measurements have been taken at currents ranging from $0.5\mu A$ to $2.0\mu A$.

To measure the effect of the triplet spin valve the resistance has been measured at fields up to $50mT$, at higher (in-plane) fields both the nickel
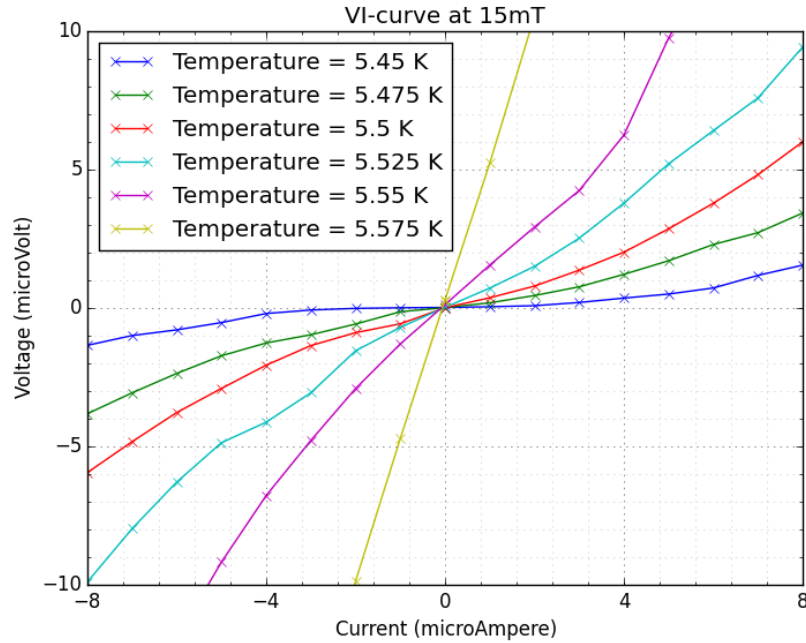
Figure 4.2: *This graph shows a set of VI-curves of BSV6 measured at a magnetic field of* 15*mT.*

and CrO_2 should both be saturated parallel to the field. Figure 4.3 shows the RT-curves for zero and maximum applied field. The curve measured at 50*mT* shows slightly higher resistances than the 0*mT*-curve, indicating a small shift in critical temperature. The T_C-shift is negative for an applied field, as expected from the theory, but can not precisely be derived from just these two RT-curves.

Another notable feature is the difference between this RT-curve (figure 4.3) and the RT-curve in figure 4.1. The curve of BSV6 does not show the second transition like the curve of BSV4 does.

To find the difference in T_C the RH-curve from figure 4.3 is used. This curve is measured at a temperature of 5.65*K*, which is part of the slope of the superconducting transitions shown the RT-curve in figure 4.3. This part of the transition is linear (figure 4.4 shows the fit) and therefore any difference in measured resistance is proportional to shift in temperature. Reading the values for resistance at different fields and comparing with the fit from figure 4.4 gives the shift in critical temperature, as shown in figure 4.4.

The biggest shift in critical temperature observed with an in-plane field applied in this sample is $\Delta T_C = 24mK$. This is about 75 times smaller than
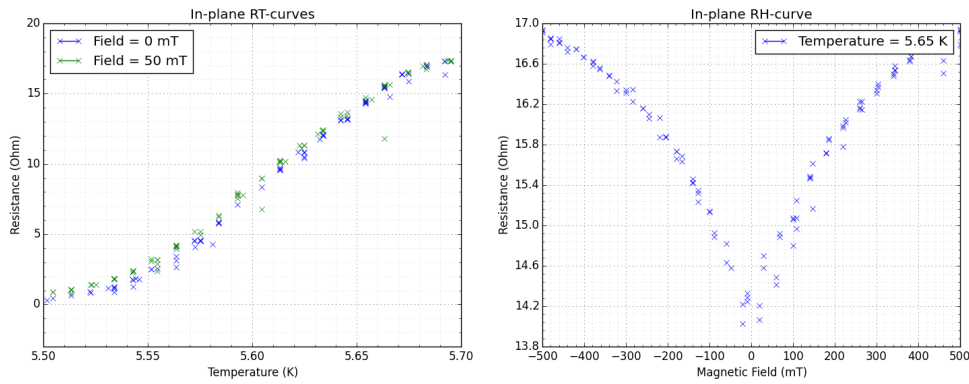
Figure 4.3: *The left graph shows two RT-curves measured at in-plane magnetic fields of $0mT$ and $50mT$. The right graph shows an RH-curve measured at a temperature of $5.65K$. Both measurements were taken with a current of $1.5\mu A$.*
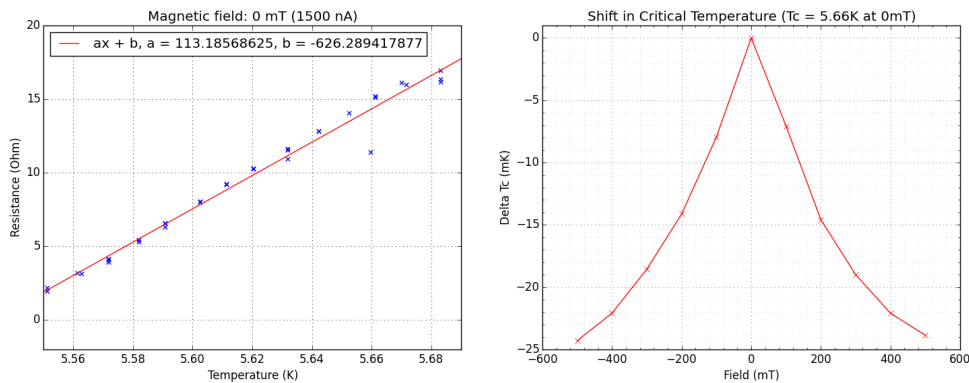
Figure 4.4: *The graph on the left shows the linearly fitted RT-curve (zero field) used to create the graph on the right, which shows field-dependency of ΔT_C.*

the $1.8K$ difference measured by Singh. Because the effect is so small it cannot be assigned to the long range triplets. This effect is likely to be just the effect of a high magnetic field on the critical temperature. In the article on the colossal proximity effect Singh shows that a T_C difference of around $100mK$ is achieved by applying a magnetic field of $250mT$ (out-of-plane) to only a MoGe layer. Because of that, this effect can not be considered due to the triplet spin valve.

The logical explanation for this is that the TSV never has been turned "on" in the first place. Further research into the ferromagnet behaviour of nickel under applied fields shows that nickel does not turn its magnetic orientation the way it was expected. The nickel bar used for this set-up

measures approximately $20\mu m \times 6\mu m \times 1.5nm$. One of the sides is significantly shorter than the others, and because of that it can be considered a film. When an out-of-plane field is applied to a nickel film the nickel responds homogeneous and quicker than the CrO_2 does. CrO_2 saturates at an out-of-plane field of around $1.5T$ and for nickel this is approximately $1.0T$ [4] while for in-plane fields this is $150mT$ for CrO_2 and $250mT$ for nickel [18]. If the field is applied in-plane the nickel does not respond homogeneously. Instead of gradually turning its magnetisation towards the direction of the field the nickel forms different domains that individually turn their magnetisations. During this divided phase it is not possible to form areas that are fully non-collinear so the TSV will stay turned "off". When the field is high enough to fully align all of these domains, the CrO_2 has turned its magnetisation too. CrO_2 is more susceptible to in-plane fields than to out-of-plane fields, so this has already happened at $50mT$.

If this is indeed the reason the found T_C-drop is this much smaller than expected applying an out-of-plane field should be an alternative way to activate the long range triplets.

4.2.2   Out-of-plane measurements

Although this device was designed to be measured with an in-plane field, the results discussed in section 4.2.1 require additional information in order to be completely understood. These out-of-plane measurements have done for two reasons. The first reason is to see whether the low ΔT_C can be explained by the different response to in-plane and out-of-plane fields. If nickel responds indeed like previously explained, applying an out-of-plane field should turn "on" the triplet spin valve. Secondly, applying an out-of-plane field can confirm the Singh's results.

Because zero field is the same for in-plane and out-of-plane field the device will be measured only with an applied field. Figure 4.5 shows the RT-curves at different fields. This time, the shift in T_C is clearly visible from these graphs. The shift is negative as expected and can simply be derived from this data, which is done in figure 4.6. To create this figure the temperatures corresponding to certain resistances at different fields have been compared with the temperature of the same resistance at zero field. The difference is ΔT_C, measured at that point of the graph. The found ΔT_C values go up to $1K$ for a field of $900mT$ and a reference resistance of 2.5Ω.

By looking at figures 4.5 and 4.6 other interesting features can be found. The change in critical temperature is not constant. Not only does it change with field, it also changes dependant of reference resistance. More pre-
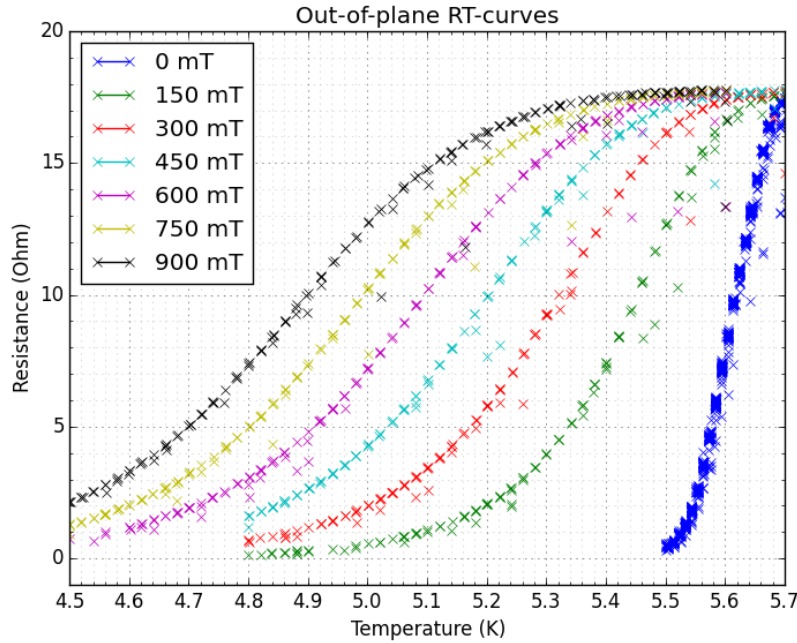
Figure 4.5: *In this graph one can find RT-curves for different applied out-of-plane fields measured at a 1.5μA current. The data for the 0mT is measured during the in-plane measurements.*

cisely: it changes dependant of place in the superconducting transition. Further in the transition (at lower temperature and resistance) the difference is larger than earlier in the transition. There can be up to a factor 3 difference (at 150mT) between 2.5Ω and 15Ω. A likely explanation for this phenomenon can be the different mechanisms that cause shifts in critical temperature. In this triplet spin valve the part of ΔT_C that is due to the actual TSV is larger at low temperature and the contribution of the magnetic field is larger at higher temperatures. This is supported by the fact that proximity effect is something that works more efficient at lower temperature. Approaching the critical field (without the proximity effect of an open TSV) only results in a displacement of the curve, so this does not change depending on the place in the curve.

These out-of-plane field measurements have shown to create a larger shift in T_C than the in-plane field measurements. This agrees with predicted behaviour of nickel films under the influence of an applied magnetic field and, more important, is in agreement with the results of Singh's colossal spin valve. Even though the record has not yet been broken, the shift in T_C has the same order of magnitude.
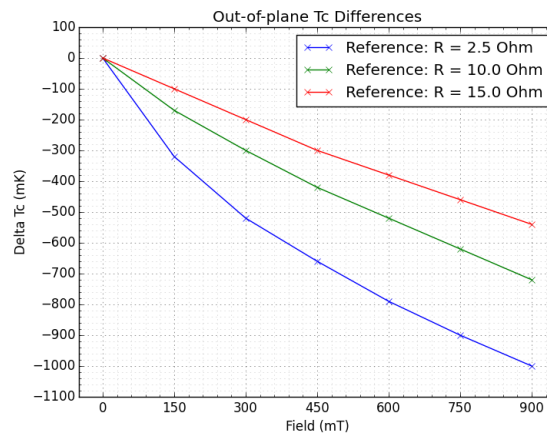
Figure 4.6: *This graph gives a quantification of the differences in critical temperature in figure 4.5 for different reference resistances.*

4.2.3 Noise

Throughout the results in sections 4.2.1 and 4.2.2 many graphs show a similar kind of noise. This noise is very consistent, as shown in figure 4.7. The noise seems to form two separate lines above and below actual data. Because this noise shows these strange extra lines in every individual raw graph it is not considered to be random noise but an artefact of the measurement set-up. This argument justifies not including this noise in the results other than this subsection.
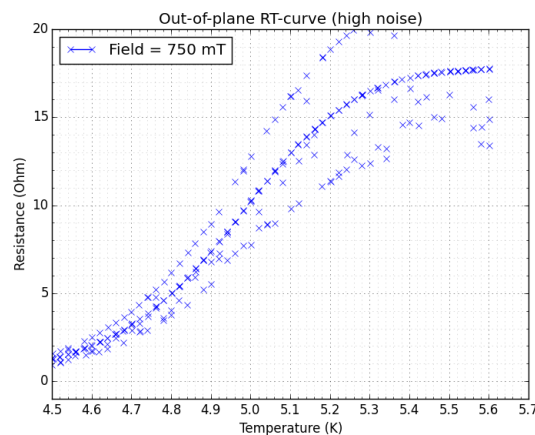
Figure 4.7: *This graph serves as an example to showcase the noise apparent during all measurements. The graph shown is made with the unfiltered data used to produce figure 4.5.*

Because the noise seems to show two extra lines similar to the desired results, one can assume that this noise is in fact not noise but data from another part of the measurement. The data used to produce figure 4.7 shows the data measured under the influence an out-of-plane field of $750mT$. For this specific measurement steps of $150mT$ are taken for the different fields. The extra lines produces by the noise look like they might belong to the data corresponding to the field of either one step higher ($900mT$) or lower ($600mT$). Figure 4.8 shows two graphs with the $900mT$ and $600mT$ results besides the $750mT$ results. Comparing the noise of the $750mT$ measurement with the desired data of the $900mT$ and $600mT$ graphs shows a very clear difference. Similar comparisons are made for every individual dataset to show that these neighbouring measurements are not the source of the noise. This second mechanism too is pure untested speculation.
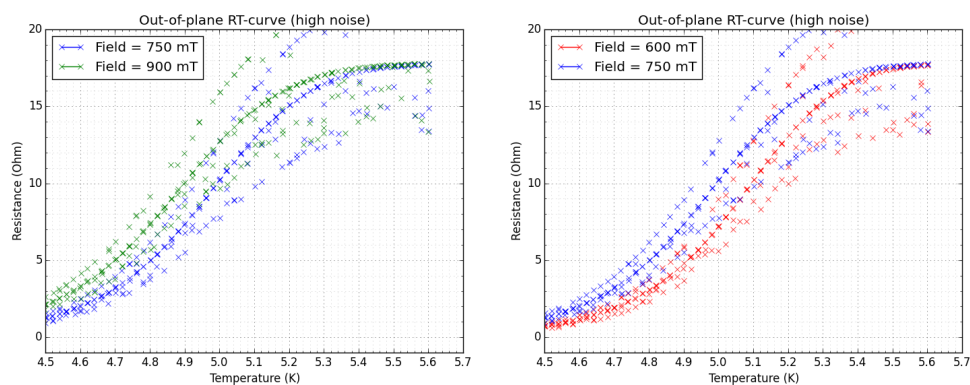
Figure 4.8: *These graphs show the noisy data of the $750mT$ measurement compared to the $900mT$ data (left) and the $600mT$ data (right).*

Though the exact source of the noise remains uncertain, there are two plausible mechanisms to which the noise can be attributed. The first and most likely mechanism is different current paths. The device has many parts that lie close to each other between which charge might build up. This is impossible parallel to superconducting parts, but not when above zero resistance. If charge does build up it might work as a capacitor that releases its charge from time to time. This would result in a short increase (or decrease, depending on the positioning of the capacitor part) in current which might explain the consistency of the noise. This, or a similar mechanism, could be the reason this noise is measured but it has not been tested. The second and very unlikely mechanism is quantisation. Perhaps part of the device creates a more-level system, however the source of such a multi-level system remains a mystery.

4.3   Uncompleted experiments

The experiments described in the previous sections leave several questions unanswered. The devices described in the following subsections were designed to help find the answers but proved more difficult to prepare. This left these devices unsuitable for measurement. This section is dedicated to describing what these samples were supposed to uncover.

4.3.1   BSV8: single ferromagnet Pt TSV

This device was designed to test whether spin-orbit coupling can be used as a mechanism for spin mixing as described in section 2.4.4 and by Jacobsen [15]. Like BSV4 (section 4.1), this device was designed around platinum because of its high spin-orbit coupling. Table 4.3 presents its design specifications.

Table 4.3: *Device information of BSV8.*

	Contains	Size
Contacts	Ag ($20nm$)	-
Bilayer	MoGe ($< 20nm$), Pt ($1.5nm$)	$3\mu m \times 12\mu m$
CrO_2	CrO_2	$100\mu m \times 10\mu m$

This device used the orthogonal design from figure 3.2 with a slightly broader trilayer bar. For the CrO_2 growth a bilayer of PMMA is used and for the plasma etching CHF_3 and argon were used (the improved recipe from section 3.2.1). The CrO_2 has been etched for $1m30s$ before sputtering platinum on top of it.

This sample had a high chance to fail from the start but ironically this had nothing to do with why it was unmeasurable. BSV8 is the only sample discussed in this thesis with only one ferromagnetic layer: the CrO_2. It was meant to see whether it was possible to make a TSV spin valve based on SO-coupling and it would have been measured while being rotated in a constant in-plane magnetic field. This field would be used to change the magnetisation of the CrO_2 with respect to the SO-vector of the platinum. During a 180°rotation the critical temperature should go down at different places. The first reason this measurement could go wrong is the magnitude of the Rashba SO-coupling compared to the Dresselhaus-coupling. Prior to this experiment there was no knowledge on how strong both of these are, and that knowledge is still lacking.

The second reason this experiment could have gone wrong is the applied magnetic field. Applying a strong magnetic field (strong enough to turn the CrO_2 in-plane) might change the structure of the platinum too. Again, there is no real knowledge on how this would affect the formation of long range triplets. Only if the Rashba- and Dresselhaus-coupling coincidently have the same magnitude in platinum and only if applying a magnetic field does not significantly change the SO-coupling this device could have given useful results regarding Jacobsen's prediction.
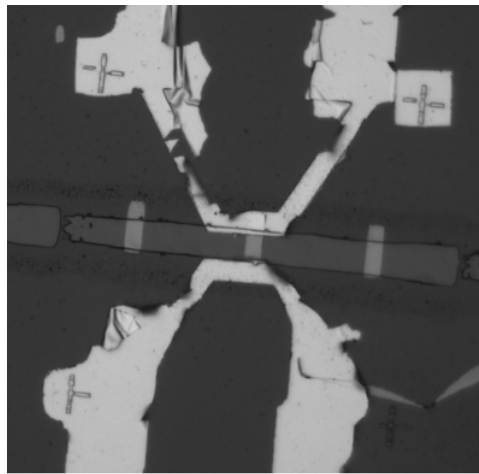
Figure 4.9: *This figure shows the contacts of BSV8. The silver wires connected to the contact pads are broken because too much metal came off due to the ultrasonication during lift-off.*

The actual reason this device was did not give the desired results is shown in figure 4.9. During the lift-off of the last layer (Ag) of BSV8 the contacts broke. This happened because the silver stuck initially too strongly to the TiO_2 substrate and needed ultrasonication to come off. This unfortunately destroyed the contacts, leaving the device useless.

4.3.2 BSV9: revised MoGe-Ni-Ag-CrO$_2$ TSV

This was the most promising of the failed devices: BSV9 was a revision of BSV6. It was designed to have the long side of its multilayer stack orthogonal to the CrO_2 easy axis (figure 3.2). In addition the ratio between the long and short side of the multilayer hase been increased to 10 : 1. The shape anisotropy of this structure ensures that the magnetisation of the nickel is aligned orthogonal to the magnetisation of the CrO_2. This way

the triplet spin valve would be turned "on" without field applied an can be turned "off" by applying an in-plane field parallel to the magnetisation of the nickel. This would confirm Singh's work and the theory of why BSV6 behaved different than expected in an in-plane field. Beside the in-plane field, this device would be unique because the critical temperature would go up under the influence of an applied magnetic field.

Table 4.4: *Device information of BSV9.*

	Contains	Size
Contacts	Ag ($20nm$)	-
Bilayer	MoGe ($20nm$), Ni ($1.5nm$), Ag($5nm$)	$0.4\mu m \times 4\mu m$
CrO$_2$	CrO$_2$	$100\mu m \times 10\mu m$

In table 4.4 the proportions of BSV9 are shown. The CrO$_2$ of BSV9 has had the same treatment and growth procedure as the CrO$_2$ of BSV8: PMMA bilayer, CHF$_3$ and Ar plasma etching and $1m30s$ CrO$_2$ etching. The wires used to connect the contact pads to the PUCK were made out of aluminium.
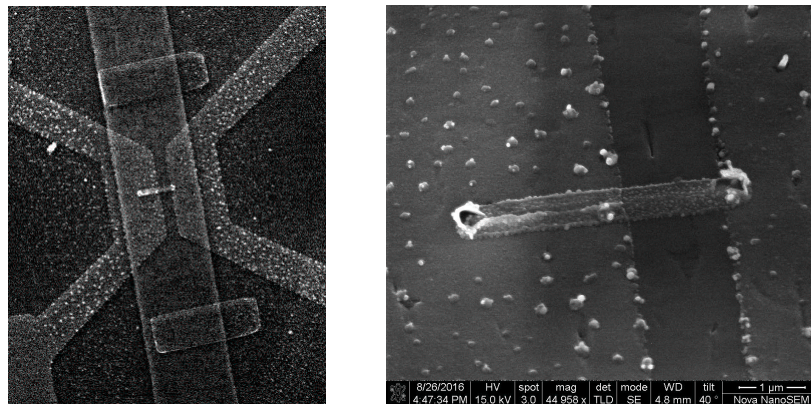
Figure 4.10: *These figures show the completed version of BSV9. The figure on the right is a close up of the middle part of the structure, it clearly shows how the silver does not properly contact the multilayer stack.*

Figure 4.10 shows one of the completed structures on BSV9. Although BSV9 was completely finished up to the wiring, a mistake happened to be made in the preparation. When measured, this device showed an incredibly high resistance at room temperature, which drastically increased when cooled down to around $10K$. This indicated that somewhere in the device a connection could not be made. Inspection by optical microscope

revealed that the silver contacts did not make contact to the MoGe-Ni-Ag trilayer. There are two likely explanations for this. The first is the lift-off procedure: the flushing with acetone might have been too rough, resulting in silver breaking. The second possibility is the e-beam current dose. For the small parts of the contacts of BSV9 (red parts in figure 3.2) a dose of $280 \frac{\mu C}{cm^2}$. For structures with sizes of less than $3nm$ (in this case the thickness of the Ag wire) in earlier devices a dose of around $340 \frac{\mu C}{cm^2}$ was used. This might result in a small layer of PMMA residue staying on the sample after developing where there should be none. When such a layer of PMMA comes of during the lift-off process it separates the silver from the trilayer. The spots on the contacts in figure 4.10 are an indication of PMMA being present underneath that layer. This would not only explain the defect on BSV9 but the breaking of the wires on BSV8 too, since the same doses are used for their contacts.

This device has unfortunately not been rebuilt, doing so could give answer to the questions that remained after the measurements on BSV6.

4.3.3   BTJ1: junction device

BTJ1 was the only Josephson junction device made for this thesis using the designs shown in figure 3.3. The purpose of these junctions is to do measurements on superconducting CrO_2 hard axis wires with different magnetic domains. A completed device similar to BTJ1 could give information about the behaviour of triplet superconductivity near domain walls and the interaction between magnetic domains and spin polarised supercurrents (perhaps even spin torque).

The device consists of horizontal (easy axis) and vertical (hard axis) CrO_2 bars, the horizontal bars with a single junction are test structures, the vertical bars with several junctions would be measured for the magnetic domains if the horizontal structures allow spin polarised currents. To fix the magnetic domains in the hard axis bars, the bars would be enhanced with notches to pin the domain walls [19]. By magnetic force microscopy and magnetic simulations the domains would be characterised and measured.

Table 4.5: Device information of BSV9.

	Contains	Size
Bilayer	MoGe ($50nm$), Ni ($1.5nm$), Ag($5nm$)	-
CrO_2	CrO_2	$100\mu m \times 1\mu m$, $1\mu m \times 100\mu m$

The fabrication of this device consists of fewer steps than the fabrication of triplet spin valves but is more sensitive when it comes to the growth of CrO_2. As table 4.5 shows, BTJ1 only has two layers: the contact pads are included in the trilayer stack. Because of this, the MoGe layer has been made somewhat thicker ($50nm$ instead of $20nm$). The CrO_2 bars made for this design had varying thicknesses for optimisation, varying from $0.5\mu m$ to $2\mu m$. The bars used for the actual junctions were $1\mu m$ thick. This sample too was connected to the PUCK with an aluminium wire.

BTJ1 was discovered to be faulty after completion. The mistake was made during the selection of the bars to build the junction on. During the inspection of the sample the different bars have been mixed up, resulting in a faulty bar being used. As figure 4.11 shows, the CrO_2 bars used are very grainy, the bars in figure 3.5 should have been used instead. Because the used bar is so grainy it is near impossible to form coherent domains or to find a current path, both destroy any supercurrents. The grains add small gaps in the bar too, creating a very high resistance, even far below the critical temperature of MoGe. This leaves the sample unusable for Josephson junctions.
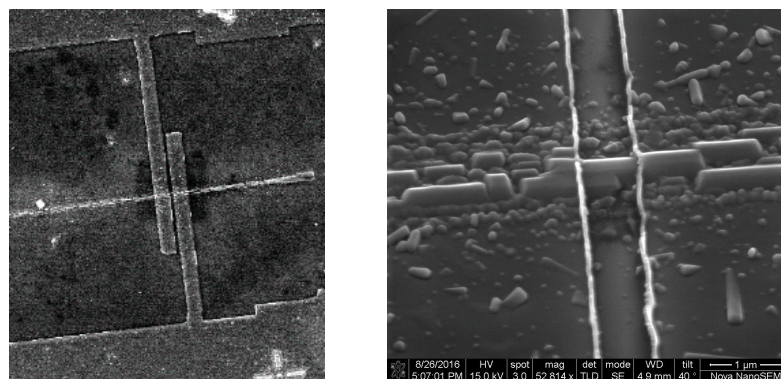
Figure 4.11: *These figures show SEM images of the junction on BTJ1. The left image shows the complete structure, the image on the right a close-up of the junction. Both figures clearly show how the CrO_2 is not properly grown.*

Chapter 5

Conclusion

The measurements on the triplet spin valve with parallel aligned CrO_2 nickel in the ground state show a large decrease in critical temperature up to $\Delta T_C = 1.0K$ when out-of-plane magnetic fields up to $900mT$ are applied. This critical temperature decrease is strongly dominated by the proximity effect of long range spin polarised triplet superconductivity. Decreasing the field to $0mT$ got the critical temperature back to its original value, confirming the long range triplets and the results measured by Singh [4]. Because the field is applied out-of-plane the critical temperature drop can not be solely the result of the long range triplets: it is enhanced by effects not related to triplets. In-plane field measurements must still be done to completely exclude these factors.

The measurements with an in-plane field show T_C-changes of a much smaller magnitude. This is likely due to the lack of control over the noncollinearity between the nickel and CrO_2. Measurements to orthogonally aligned nickel-CrO_2 triplet spin valves should be done in order to be completely conclusive about the in-plane field response of these triplet spin valves.

The results regarding spin-orbit coupling and Josephson junctions do not lead to any conclusions, they are too incomplete to make any significant comments.

Chapter 6

Outlook

The measurements of the parallel oriented nickel-CrO_2 triplet spin valves leave uncertainty about the response of TSV's under the influence of in-plane magnetic fields. Measurements on orthogonally aligned nickel-CrO_2 TSV's should allow to find the same large critical temperature drops that are found in the out-of-plane measurements. These changes in critical temperature would result in an effect that is only due to the proximity effect of long range triplet superconductivity, excluding any not triplet related effects. In addition, out-of-plane field measurements can be done to find how much the long range triplets contribute to the found $1.0K$ critical temperature drop in the parallel out-of-plane measurements.

Measurements to the predictions Jacobsen [15] can be done to find insights on the effects of spin-orbit coupling in triplet spin valves. For the effect of spin-orbit coupling in the spacer layer devices similar to BSV6 and BSV4 can be done. Using platinum or gold as spacer layers should be an easy way to confirm or reject the theory. For confirmation of the possible single ferromagnet TSV's more research should be done to the magnitudes of the Rashba and Dresselhaus SO-coupling. If not, the experiment would be very likely to be inconclusive.

Josephson junctions on CrO_2 with domain walls seem very promising after the results of the parallel nickel-CrO_2 triplet spin valve. The devices should first be tested for single domain CrO_2 before trying multiple domains.

Chapter 7

Acknowledgements

First of all I would like to thank my daily supervisor MSc Kaveh Lahabi for all of his guidance and help. Beside being an understanding tutor he happily stayed until deep in the night (or morning) to help me out with whatever problem happened to occur.

Secondly I would like to thank my supervisor Prof. Dr. Jan Aarts for watching over the project and for lending me his vast knowledge about superconducting systems.

In the third place I would like to thank my second corrector Dr. Peter Gast for taking the time to read and rate this thesis and my work.

Then I would like to thank the technicians Dr. Ir. Marcel Hesselberth, Dr. Ir. Anne-France Beker and Thomas Mechelson for always making time to help me out with the technical difficulties I could not solve by myself.

After that I would like to thank Dr. Amrita Singh, Willem Tromp and Bart Woltjes for their close collaboration and help.

Lastly I would like to thank the whole Magnetic and Superconducting Materials group for all of their support and kindness, I have had a great time being part of your team!

References

[1] P. V. Leksin, N. N. Garif'Yanov, I. A. Garifullin, Y. V. Fominov, J. Schumann, Y. Krupskaya, V. Kataev, O. G. Schmidt, and B. Büchner, *Evidence for triplet superconductivity in a superconductor-ferromagnet spin valve*, Physical Review Letters **109**, 1 (2012).

[2] J.Y. Gu, C.-Y. You, J. S. Jiang, J. Pearson, Ya. B. Bazaliy and S. Bader, *Magnetization-Orientation Dependence of the Superconducting Transition Temperature in the Ferromagnet-Superconductor-Ferromagnet System: CuNi/Nb/CuNi*, Physical Review Letters **89**, 157004 (2002).

[3] X. L. Wang, A. Di Bernardo, N. Banerjee, A. Wells, F. S. Bergeret, M. G. Blamire, and J. W. A. Robinson, *Giant triplet proximity effect in superconducting pseudo spin valves with engineered anisotropy*, Physical Review B - Condensed Matter and Materials Physics **89**, 3 (2014).

[4] A. Singh, S. Voltan, K. Lahabi, and J. Aarts, *Colossal Proximity Effect in a Superconducting Triplet Spin Valve Based on the Half-Metallic Ferromagnet CrO2*, Physical Review X **5**, 021019 (2015).

[5] M. Tinkham, *Introduction to Superconductivity*, second edition, 1996.

[6] M. Eschrig, *Spin-polarized supercurrents for spintronics: a review of current progress*, Reports on Progress in Physics **78**, 95 (2015).

[7] M. Eschrig, *Spin-polarized supercurrents for spintronics*, Physics Today **64**, 43 (2011).

[8] J. Linder and J. W. A. Robinson, *Superconducting spintronics*, Nature Physics **11**, 307 (2015).

[9] M. Houzet and A. I. Buzdin, *Long range triplet Josephson effect through a ferromagnetic trilayer*, Physical Review B - Condensed Matter and Materials Physics **76**, 1 (2007).

[10] J. M. D. Coey and M. Venkatesan, *Half-metallic ferromagnetism: Example of CrO 2 (invited)*, Journal of Applied Physics **91**, 8345 (2002).

[11] S. P. Lewis, P. B. Allen, and T. Sasaki, *Band Structure and Transport Properties of Single-Crystal Graphite*, J. Phys. Chem. Solids **8**, 29 (1996).

[12] B. Josephson, *Possible new effects in superconductive tunnelling*, Physics Letters **1**, 251 (1962).

[13] P. W. Anderson and J. M. Rowell, *Probable observation of the Josephson superconducting tunneling effect*, Physical Review Letters **10**, 230 (1963).

[14] R. S. Keizer, S. T. B. Goennenwein, T. M. Klapwijk, G. Miao, G. Xiao, and A. Gupta, *A spin triplet supercurrent through the half-metallic ferromagnet CrO2.*, Nature **439**, 825 (2006).

[15] S. H. Jacobsen, J. A. Ouassou, and J. Linder, *Critical temperature and tunneling spectroscopy of superconductor-ferromagnet hybrids with intrinsic Rashba-Dresselhaus spin-orbit coupling*, Physical Review B - Condensed Matter and Materials Physics **92**, 1 (2015).

[16] A. Singh, C. Jansen, K. Lahabi, and J. Aarts, *Growth of half-metallic CrO 2 nanostructures for superconducting spintronic applications*, Arxive , 1 (2016).

[17] J. Robinson, *A Boost for Superconducting logic*, Physics **8**, 49 (2015).

[18] W. P. Sterk, *Magnetisation characteristics of noncollinear ferromagnetic bilayers*, Bachelor thesis, Leiden University, 2015.

[19] J. B. Woltjes, *Domain Walls in CrO2 nanowires*, Bachelor thesis, Leiden University, 2016.

[20] M. Isasa, E. Villamor, L. E. Hueso, M. Gradhand, and F. Casanova, *Temperature dependence of spin diffusion length and spin Hall angle in Au and Pt*, Physical Review B - Condensed Matter and Materials Physics **91**, 15 (2015).